JOURNAL OF AIRCRAFT
Vol. 40, No. 2, March–April 2003

Structured and Unstructured Computations on the DLR-F4 Wing–Body Configuration

M. Rakowitz* and B. Eisfeld†
DLR, D-38108 Braunschweig, Germany
D. Schwamborn‡
DLR, D-37073 Göttingen, Germany
and
M. Sutcliffe§
Airbus Deutschland GmbH, D-28183 Bremen, Germany

The accuracy of the DLR structured and unstructured computational fluid dynamic (CFD) codes in predicting aircraft forces and moments on a wing–body configuration at subsonic and transonic speeds is investigated. The computations form the contribution of the DLR and Airbus Deutschland to the AIAA CFD Drag Prediction Workshop (DPW) in June 2001. By the use of a combination of a high-quality grid, low levels of artificial dissipation, and an advanced turbulence model, the structured code (FLOWer) was able to predict both qualitatively and quantitatively the experimentally measured drag, lift, and pitching moments. Compared to the structured methods, the total time for grid and solution generation is significantly reduced with the unstructured approach. Nevertheless, in its current implementation, the unstructured code (TAU) was found to be less accurate in predicting forces and moments for the F4 case, although qualitatively the results were good.

Nomenclature

C_D, C_L	=	drag and lift coefficients
C_M, C_P	=	pitching moment and pressure coefficients
f_0	=	grid-converged solution (Richardson extrapolation)
f_1	=	solution on fine grid
f_2	=	solution on next coarser grid
$k2, k4$	=	second- and fourth-order dissipation coefficients
Ma	=	freestream Mach number
M_D	=	drag divergence Mach number
p	=	theoretical or observed order of accuracy
r	=	grid refinement ratio
α	=	angle of attack
ζ	=	eigenvalue dissipation scaling factor

Introduction

THIS work comprises the contribution of the DLR and Airbus Deutschland GmbH to the AIAA Drag Prediction Workshop (DPW) in Anaheim, California, 9–10 June 2001 (URL: http://ad-www.larc.nasa.gov/tsab/cfdlarc/aiaa-dpw/index.html). The test configuration is the DLR-F4 wing–body configuration[1] flying at subsonic through transonic speeds ($Re = 3e6$). The focus of the workshop is drag prediction accuracy using a statistical analysis of the contributed results for the test cases:

1) Case 1 is a single point with provided grids at $Ma = 0.75$ and $C_L = 0.5$.

2) Case 2 is a drag polar for $Ma = 0.75$ and $\alpha = -3$–2 deg (increments of 1 deg) using self-generated grids.

3) Cases 3 and 4 are Ma/C_L matrices (drag rise curves) with Mach $= 0.5 - 0.8$ and $C_L = 0.4$, 0.5, and 0.6, again using self-generated grids.

The computations for the workshop are in fully turbulent mode and are compared to experimental results[1] with fixed transition. Additional work was carried out to investigate the effect of turbulence modeling, transition, artificial dissipation, different grids, and mesh refinement. This paper investigates how the more and more popular unstructured CFD methods involving hybrid grid technology compare to established structured methods in terms of the level of accuracy, automation, and performance.

CFD Software

The unstructured TAU[2] code, the structured FLOWer[3] code and the structured grid generator MegaCads[4] have been developed primarily by the DLR within the German CFD initiative MEGAFLOW,[5] which is a cooperative effort of the DLR, aircraft industry, and several universities. The software is used extensively for aerodynamic design and research activities in the aircraft industry and the DLR.

Structured Grid Generation

The DLR structured multiblock grid (seven blocks) has a C–O–H topology for high resolution. A number of geometrical modifications compared to the standard F4 geometry are made to simplify grid generation. The trailing edge of the wing is closed with Bézier splines from $(x/c) = 90\%$ onward,[6] and the fuselage plug is slightly altered to allow the C block around the wing. It will be shown that this geometry modification has a negligible effect on the results. The grid generation takes advantage of the replay capability of MegaCads. Important parameters like cell numbers and spacings are controlled by variables that allow fast modifications to grids. This is used for the generation of three computational meshes (3.5*e*6, 5*e*6, and 18.7*e*6 points). Cell numbers and placement are chosen based on experience gained by Rakowitz[7] with the aim of achieving a sufficient resolution on all grids. The majority of computations use the 3.5*e*6

Presented as Paper 2002-0837 at the AIAA 40th Aerospace Sciences Meeting and Exhibit, Reno, NV, 14 January 2002; received 25 February 2002; revision received 18 September 2002; accepted for publication 4 October 2002.

*Research Scientist, Transport Aircraft, Institute of Aerodynamics and Flow Technology, Lilienthalplatz 7; Mark.Rakowitz@dlr.de.

†Research Scientist, Numerical Methods, Institute of Aerodynamics and Flow Technology, Lilienthalplatz 7; Bernhard.Eisfeld@dlr.de.

‡Head of Numerical Methods, Institute of Aerodynamics and Flow Technology, Bunsenstrasse. 10; Dieter.Schwamborn@dlr.de.

§Research Scientist, Aerodynamic Design and Data, Hünefeldstrasse 1-5; Mark.Sutcliffe@airbus.com.

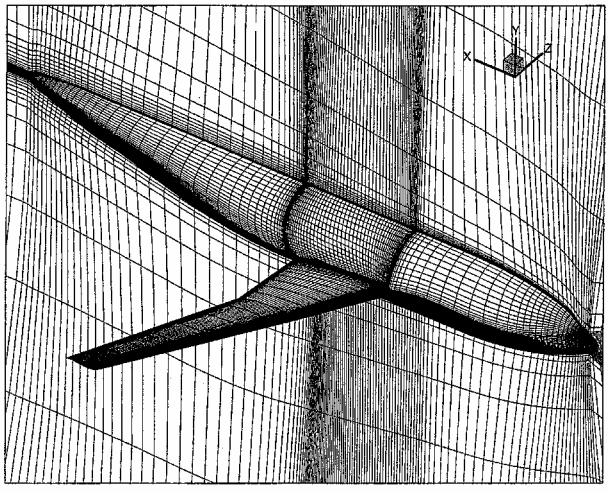

a) Structured MegaCads grid (every second grid line shown)

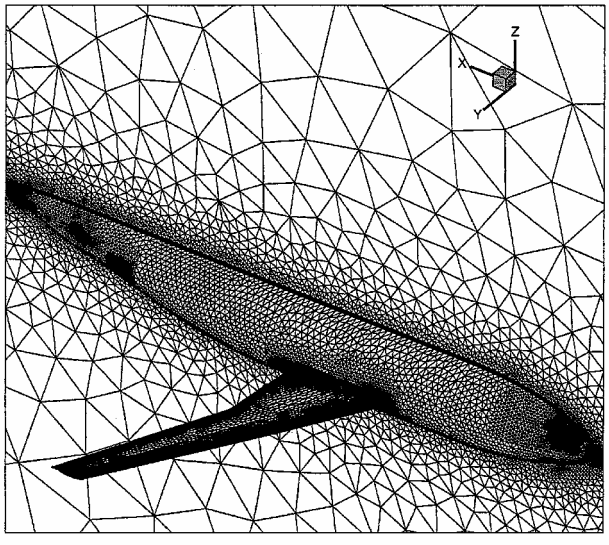

b) Hybrid Centaur^{TM} grid

Fig. 1 Structured and unstructured DLR grids.

points grid. The finer grids are used to show the influence of mesh refinement on the computational results. The cell distribution in the 3.5*e*6 points mesh is chosen to have at least 20 cells normal to the wing surface in the boundary layer at all angles of attack of the polar in case 2, and the height of the first layer is 0.001 mm. The far-field distance is 70 times the reference chord length or eight times the fuselage length in every direction. Figure 1a shows a cutaway of the F4 structured multiblock grid.

Structured Flow Solver FLOWer

The FLOWer code solves the three-dimensional compressible Reynolds-averaged Navier–Stokes (RANS) equations in integral form. Turbulence is modeled by either algebraic or transport equation models. Here the Wilcox–$k\omega$,[8] the $k\omega$–linearized algebraic stress (LEA),[9] and the Spalart–Allmaras[10] (SA), or SA with Edwards modification (SAE) (see Ref. 11) models are used. The spatial discretization uses a central cell-centered finite volume formulation. Dissipative terms are explicitly added to damp high-frequency oscillations and to achieve sufficiently sharp resolution of shock waves. The dissipative operator comprises second- (k2) and fourth (k4) order differences scaled by the largest eigenvalue following Jameson et al.[12] and Martinelli and Jameson.[13] Some computations use a small amount of matrix dissipation.[14] On smooth meshes, the scheme is second-order accurate in space. Time integration is carried out by an explicit hybrid multistage Runge–Kutta scheme. For steady-state calculations, the integration is accelerated by local time stepping and implicit residual smoothing. These techniques are embedded in a multigrid algorithm. The code allows two dummy layers around each block to maintain second-order accuracy in space at block intersections.

Unstructured Grid Generation

The DLR unstructured hybrid grids are generated using the Centaur^{TM} software package provided by CentaurSoft. The nominal grid contains 24 prism layers for resolution of the boundary layer. The initial spacing away from the wall is 0.001 mm, which is based on obtaining a y^+ of approximately one. (The reference chord length is 141.2 mm.) A prismatic stretching factor of 1.4 is used. An O-topology prismatic grid is used around the wing to include the finite thickness trailing edge. The trailing edge is resolved with four cells in the vertical direction, yielding a grid with a total of 1.7*e*6 points (4.6*e*6 cells). The far field is positioned at ± 130 times the reference chord length, or ± 15 times the fuselage length in all directions. Figure 1b depicts the surface and symmetry plane grid. Numerous variations on the standard grid are generated to investigate the influence of the grid on the numerical results. Further details regarding these grids and the results are provided in the section "Parametric Study."

Unstructured Flow Solver TAU

The TAU code solves the three-dimensional compressible RANS equations on hybrid grids. The initial/adapted grid is input into the preprocessing module, which computes dual grids using an edge-based data structure (independent of the element types in the hybrid grid). Coarse grids for the multigrid algorithm are constructed recursively by agglomerating the control volumes at the finer grid level. For parallel computation, the dual grids (fine grid and coarse grid levels) are partitioned into a number of domains, each corresponding to a processor. The flow solver is based on a finite volume scheme integrating the RANS equations. The flow variables are stored in the centers of the dual grid, that is, the vertices of the primary grid. In this study, the inviscid fluxes are calculated by employing a central method with scalar dissipation. (Standard settings are $\zeta = 0.5$, $k2 = \frac{1}{2}$, and $k4 = \frac{1}{64}$.) The gradients of the flow variables are determined by a Green–Gauss formula. The viscous fluxes are discretized using central differences. The compressible flow solver employs an explicit multistep Runge–Kutta scheme for the discretization of the temporal gradients. To accelerate the convergence to steady state, residual smoothing and a multigrid technique (4*w* for this study) are employed. The turbulence model used in this study is the one-equation SA model.[10] The adaptation module allows for local refinement of the hybrid grid based on a sensor derived from the flow solution. In this study, the sensor was based on a combination of the total pressure, total enthalpy, velocity, and density. The adaptation module also allows the redistribution of points in the structured prismatic/hexahedra sublayers for an improved boundary-layer resolution. This adaptation feature was set to obtain a y^+ spacing of 1 at the wall.

Workshop Results

The computational results for the four test cases are compared to the experimental results obtained in three different wind tunnels, the High Speed Wind Tunnel (HST) of the National Aerospace Laboratory (NLR), the ONERA-S2MA wind tunnel of the ONERA, and the 8 foot Wind Tunnel of the Defence Research Agency (DRA).

Case 1

Case 1 involves computations using grids provided by the workshop committee (to be called the DPW grids) for $Ma = 0.75$ and $C_L = 0.5$. The structured multiblock DPW grid with 3.2*e*6 points has an O topology around the wing. The unstructured DPW tetrahedra grid has 1.7*e*6 points. The unstructured boundary-layer grid is generated using the advancing-layers method,[15] which produces highly stretched and ordered tetrahedral cells marching in a direction normal to the surface. This effectively produces an unstructured grid with an O topology around the wing in the boundary-layer region. The FLOWer computations use scalar dissipation with the following

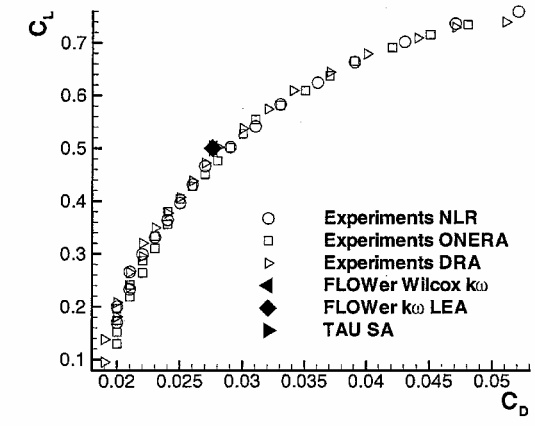

a) $C_L(C_D)$

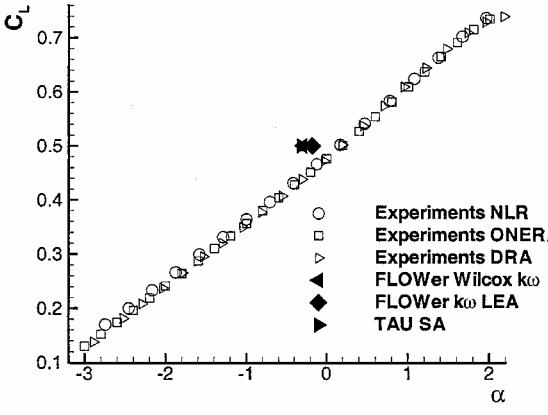

b) $C_L(\alpha)$

Fig. 2 Provided grids, case 1 ($C_L = 0.5$).

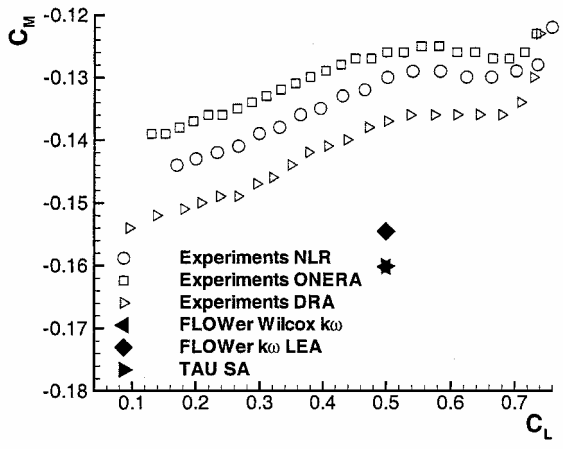

a) $C_M(C_L)$

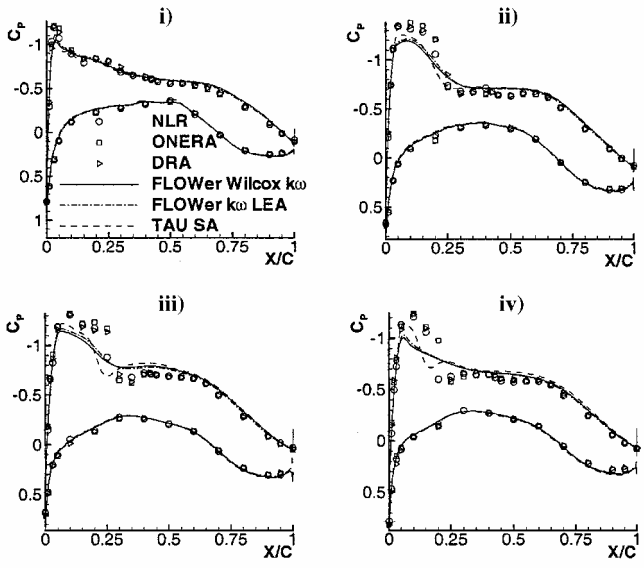

b) $C_P(x/c)$: η = i) 0.185, ii) 0.331, iii) 0.512, and iv) 0.844

Fig. 3 Provided grids, case 1 ($C_L = 0.5$).

settings: $\zeta = 0.67$, $k2 = \frac{1}{4}$, and $k4 = \frac{1}{64}$. The unusually high value for ζ is required to obtain a solution with the DPW grid; lower values lead to solution divergence. This issue is addressed further in the section "Parametric Study." For the TAU result, the standard dissipation settings described in "Unstructured Flow Solver TAU" are used.

Figure 2a shows FLOWer results using the Wilcox–$k\omega$ (Ref. 8) and the $k\omega$–LEA turbulence model and a TAU computation using the SA model.[10] Although two grids and three different turbulence models are used the predicted drag levels are almost identical. Note that fixed transition[1] was used in the experiments, whereas the computations were fully turbulent. Computations investigating the influence of transition are presented later in the section "Parametric Study."

Figure 2b depicts $C_L(\alpha)$. All three computations underpredict the angle of attack required for $C_L = 0.5$ (0.2 deg). The FLOWer Wilcox–$k\omega$ (Ref. 8) (−0.30 deg) and the TAU SA (Ref. 10) (−0.32 deg) results are almost identical, with a slightly better result coming from the FLOWer $k\omega$–LEA calculation (−0.18 deg). The same conclusions can be drawn for the pitching moment coefficient displayed in Fig. 3a. The result from the $k\omega$–LEA computation lies slightly closer to the experimental results; however, all results are quite removed from the experiment.

Figure 3b depicts $C_P(x/c)$ at four spanwise stations on the wing at $C_L = 0.5$. The agreement with the experiments at $\eta = 0.185$ is good for all three computations. Only the suction peak in the computations is too low. When moving toward the outer section of the wing, the agreement with experiment gradually declines. At section $\eta = 0.331$ and 0.512, the FLOWer results have a very smeared shock. The TAU result is not as smeared and has a higher rooftop level, closer to the experiments, but the shock position is too far forward. At $\eta = 0.844$, the FLOWer results show no shock at all. The pressure distributions can be summarized as having a pressure level in the recovery region after the smeared shock that is generally above the experiments, combined with a lower than measured suction peak. To conclude, the apparently good correlation of drag to the experiment for all computations is due to a cancellation of errors, highlighted by the differences between experiment and calculation for lift, moment, and the pressure distributions. To investigate the influence of the coupling between grid and solver on these results, self-generated grids are used for case 2.

Case 2

The best FLOWer and TAU results for the complete range of angles of attack are presented using grids generated in-house at the DLR. The FLOWer computations use a grid with 3.5e6 points (see "Structured Grid Generation") combined with a minimum amount of artificial dissipation (87.5% scalar dissipation, 12.5% matrix dissipation, and scaling factor due to largest eigenvalue $\zeta = 0.2$, $k2 = \frac{1}{4}$, and $k4 = \frac{1}{64}$) and the $k\omega$–LEA turbulence model. The TAU results use an initial grid containing 1.7e6 points (see "Unstructured Grid Generation"), which is adapted once at each angle of attack, yielding grids with 2.4e6 points (+40%). In the adaption stage, a $y^+ = 1$ adaption of the prismatic grid is also performed. The one-equation SA[10] turbulence model is used, combined with the standard settings for artificial dissipation (see "Unstructured Flow Solver TAU"). A detailed parametric study is presented in the following section, "Parametric Study."

The fully turbulent FLOWer computations overpredict the measured drag curve (Fig. 4a) by approximately 20 drag counts. Note that the inclusion of transition in the calculation reduces the predicted drag by approximately 14 drag counts (see "Influence of Transition and Mesh"), reducing the drag overprediction to approximately six drag counts. The results from the unstructured fully

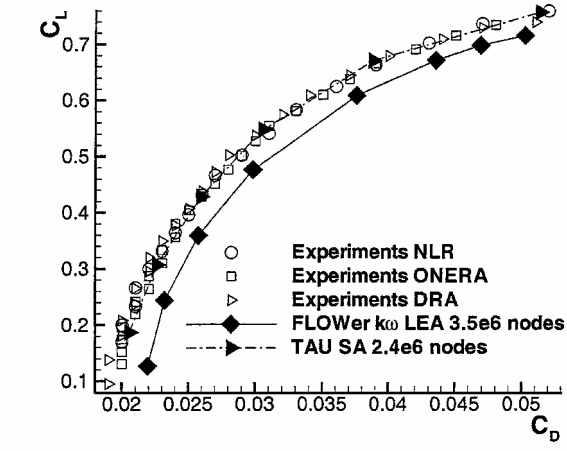

a) $C_L(C_D)$

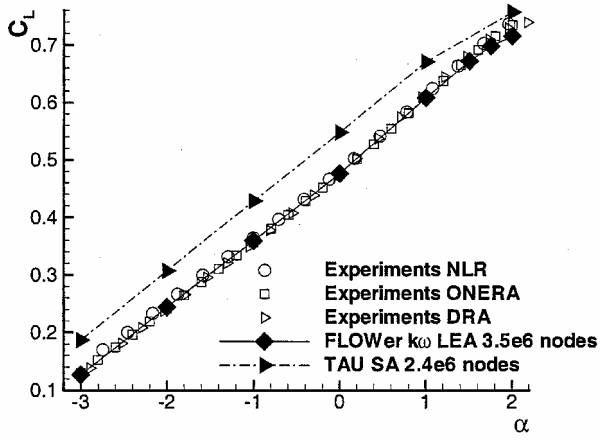

b) $C_L(\alpha)$

Fig. 4 DLR grids, case 2.

turbulent computations with TAU lie exactly on the experimental results. However, as is the case for the structured computations, including transition reduces the predicted level of drag, in this case by approximately 10 drag counts.

The calculated lift curves are shown in Fig. 4b. The FLOWer lift curve matches the experiment very well, even in the nonlinear region above $\alpha = 0.5$ deg, with a slight deviation in the region $\alpha = 1.5$–2 deg. In comparison, the lift from the TAU calculations overpredicts that of the experiment by approximately 15% over almost the whole range of angles. Figure 5a again shows good agreement between the FLOWer and experimental results for the pitching moment, particularly given the experimental scatter between the different wind-tunnel facilities. The changes in slope of the pitching moment curve are also captured very well. Such an agreement is only possible when the computed pressure distributions agree very well with the experiment, as can be seen in Fig. 5b. The TAU results, as can be expected from the pressure distributions, significantly overpredict the pitching moments, accompanied by less qualitative agreement in the slope. To summarize, the TAU results for case 2 on the DLR grid are very similar to those obtained with the DPW grid for case 1. The significantly improved agreement of the FLOWer computations with experiment is achieved by using minimal artificial dissipation (at the cost of robustness, that is, convergence is slow) and by the generation of a more suitable grid, combined with an advanced turbulence model.

Case 3 and 4

The results from the drag rise curve calculations for cases 3 and 4 are presented in the form of the drag divergence Mach number M_D at $\mathrm{d}(C_D)/\mathrm{d}(Ma) = 0.1$ in Table 1. M_D was evaluated separately for the three sets of experimental results using splines and then averaged. For $C_L = 0.4$, no M_D could be evaluated because the calculations

Table 1 Drag divergence Mach numbers

C_L	M_D experiment	M_D FLOWer	M_D TAU
0.5	0.784	0.783 (−0.1%)	0.780 (−0.5%)
0.6	0.767	0.774 (+0.9%)	0.774 (+0.9%)

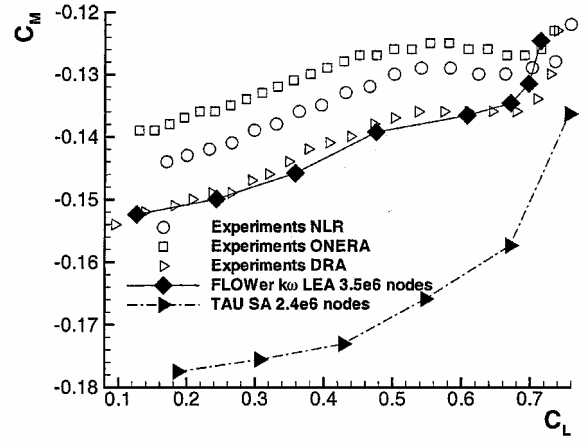

a) $C_M(C_L)$

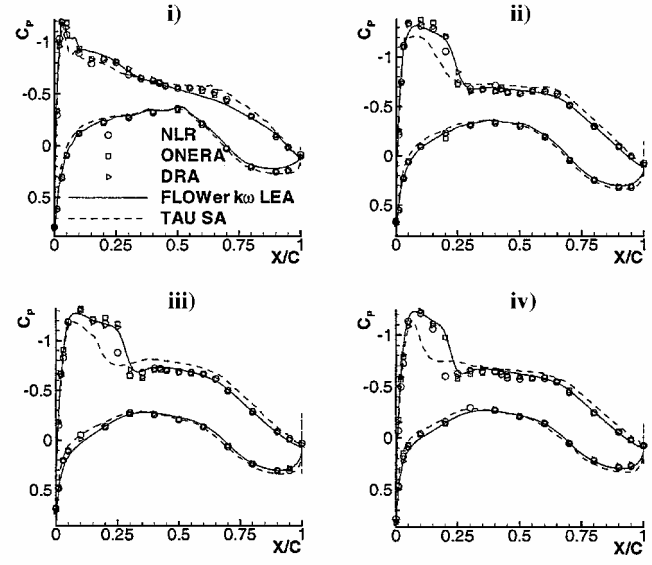

b) $C_P(x/c)$: η = i) 0.185, ii) 0.331, iii) 0.512, and iv) 0.844

Fig. 5 DLR grids, case 2, $C_L = 0.5$.

were only performed up to $Ma = 0.8$. The experimental drag divergence number at $C_L = 0.4$ was 0.802. The drag divergence Mach numbers of both TAU and FLOWer are close to the experiment (to within ±1%). For the evaluation of M_D, the accuracy of the slope is crucial. The results from this study suggest that the slope seems to be relatively insensitive to the grid, solution quality, and the type of flow solver.

The drag rise curves from FLOWer and TAU for $C_L = 0.5$ are depicted in Fig. 6. Because the drag rise curves are qualitatively very similar for all three lift coefficients, the results for the other lift coefficients are omitted. The results from the TAU computations agree qualitatively and quantitatively well with the experimental values. The FLOWer results overpredict the amount of drag; however, the slope is very similar between experiment and computations, as is evident in the good prediction of M_D. This offset of the FLOWer results is due to a higher level of artificial dissipation stemming from setting ζ to 0.67 (for case 2 a value of 0.2 was used). This higher ζ setting improves the robustness of the automatic target C_L option of FLOWer used to obtain these results. Also recall that the inclusion of transition would reduce the overall level of drag seen in Fig. 6 (lowering the drag rise curves), but would have little or no effect on the computed drag divergence Mach numbers in Table 1.

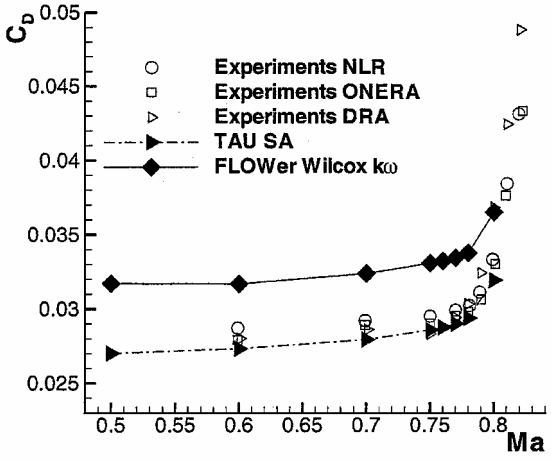

Fig. 6 Drag divergence, $C_L = 0.5$.

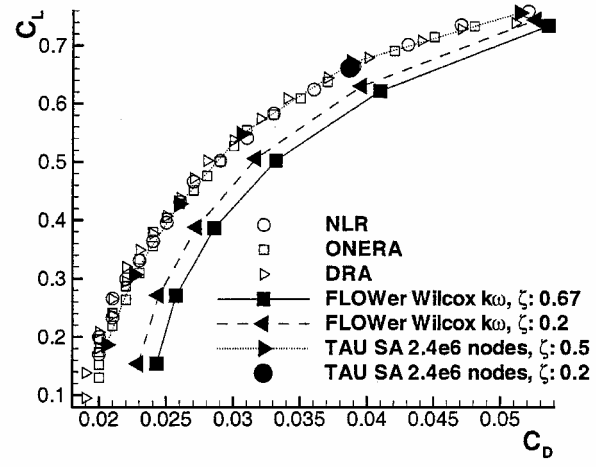

a) Influence of ζ on $C_L(C_D)$

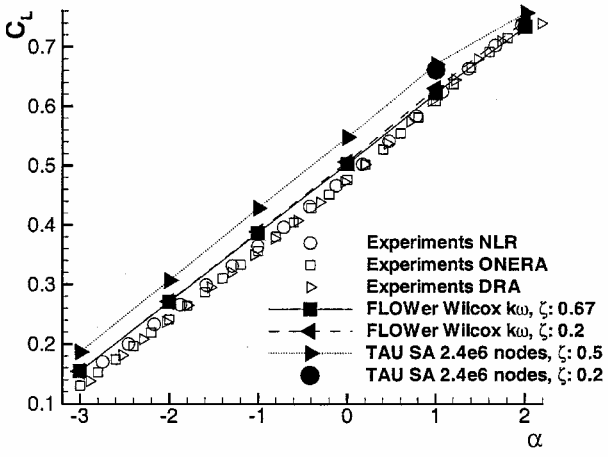

b) Influence of ζ on $C_L(\alpha)$

Fig. 7 DLR grids.

Parametric Study

In the preceding section, the best results for both the structured grid and unstructured grid computations are presented. The current section summarizes an extensive parametric study done to investigate the influence of numerous parameters on the computation results. Included in this study are 1) artificial dissipation, 2) the turbulence model, 3) transition and mesh quality, 4) flow solver and geometry modifications, and 5) mesh refinement and grid extrapolation.

Influence of Artificial Dissipation

In Figs. 7a–8b the influence of the scaling parameter of the artificial dissipation due to the largest eigenvalue ζ on the TAU and FLOWer results on DLR grids is investigated. For the FLOWer computations 100% scalar dissipation is used ($k2 = \frac{1}{4}$ and $k4 = \frac{1}{64}$) with the Wilcox–$k\omega$ turbulence model.[8] For TAU the standard settings (see "Unstructured Flow Solver TAU") are used. Figure 7a shows a decrease of approximately 5% in the FLOWer drag polar when ζ is reduced from 0.67 to 0.2. This increase in accuracy causes a decrease of robustness; thus, the computation converges more slowly. The changes in the TAU results obtained from lowering ζ from 0.5 (standard setting) to 0.2 for $\alpha = 1$ degree are less pronounced. The changes in drag (−0.4%), lift (−1.4%), and pitching moment (+3.1%) suggest that the results from the unstructured computations are much less sensitive to this parameter. The structured DLR grid has cells at the surface of the geometry with a much higher aspect ratio than TAU in the spanwise direction. This higher aspect ratio is reflected in the directional eigenvalues, and, hence, the influence of the scaling factor ζ on the dissipation is more pronounced. Figure 7b shows that for lift over angle of attack the impact of ζ on the FLOWer results is much smaller. The influence of this parameter on the pitching moment curves (Fig. 8a) for both solvers is relatively small compared to the variation in the experimental results in the different wind tunnels. Figure 8b shows the $C_P(x/c)$ at four wing sections for the FLOWer results with the different ζ values at $\alpha = 0$ deg. The impact of a lower ζ on the pressure distributions is small and increases in outboard direction with a higher rooftop level, a steepening shock, and an improved pressure recovery after the shock.

Influence of Turbulence Modeling in FLOWer

Here, three turbulence models, the Wilcox–$k\omega$,[8] $k\omega$–LEA,[9] and SAE (see Ref. 11) are compared using FLOWer computations on the DLR 3.5e6 points grid. All parameter settings are the same as for the FLOWer results for case 2. Only ζ for the SAE computation is increased to 0.5 because it will be compared to TAU computations using $\zeta = 0.5$ later. Because the FLOWer results are sensitive to ζ due to the high aspect ratio cells at the surface, the SAE results in Figs. 9a–10a are influenced most noticeably in the drag and moment curves with parallel shifts. Because the best overall agreement with experiment is achieved with the $k\omega$–LEA model, the other two sets of computations are compared to these results. Figure 9a shows that the drag polars of the two $k\omega$ models are on top of each other for C_L of less than 0.5. For higher C_L, the Wilcox–$k\omega$ (Ref. 8) result diverges slightly and is not parallel to the experiments any more. The SAE (see Ref. 11) computations have a parallel offset to higher drag caused by the higher ζ, and, from Fig. 7a, it can be concluded that with a value of $\zeta = 0.2$ the SAE and the $k\omega$–LEA model results would be much closer.

Figure 9b shows that the Wilcox–$k\omega$ (Ref. 8) results have an almost parallel offset to higher lift compared to the $k\omega$–LEA model. The SAE (see Ref. 11) model computations agree well with $k\omega$–LEA for $\alpha = -3$–0 deg and then underpredict the lift for higher angles of attack. Figure 7b shows that for lift over angle of attack, the influence of ζ is negligible. The moment curve for the Wilcox–$k\omega$ (Ref. 8) results (Fig. 10a) has a large offset to lower C_M. However the qualitative changes in the slope seen in the experiments have been well captured. The SAE model (see Ref. 11) compares well to $k\omega$–LEA for C_L of less than approximately 0.47 and then diverges to higher C_M, without qualitative agreement of the slope for higher C_L values. Figure 10b shows that the C_P distributions for $\alpha = 0$ deg of the inner two wing sections differ mainly in the pressure recovery region on the upper side of the wing, with the Wilcox–$k\omega$ model[8] producing the highest lift at the same angle of attack. The outer three sections show a difference in shock position with the shock position with the SAE (see Ref. 11) model lying slightly forward of the $k\omega$–LEA result and with the Wilcox–$k\omega$ (Ref. 8) result lying further rearward.

Influence of Transition and Mesh

In this section, the influence of transition and mesh quality on the computed results is investigated. Complete polars for case 2

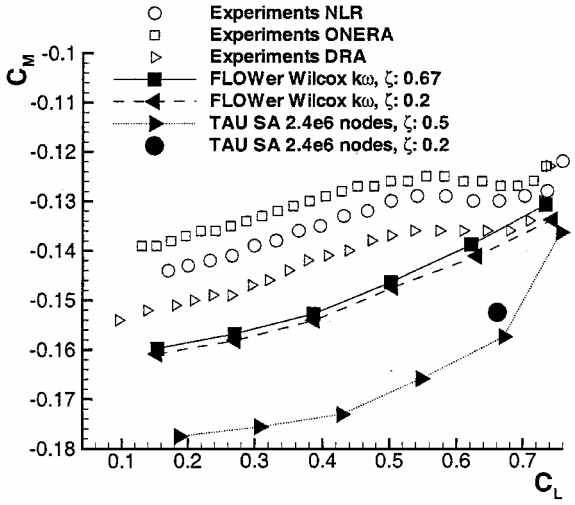

a) Influence of ζ on $C_M(C_L)$

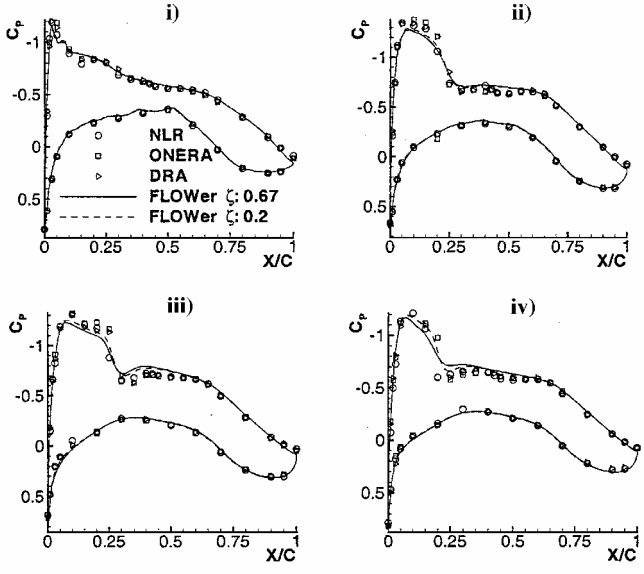

b) Influence of ζ on $C_P(x/c)$: η = i) 0.185, ii) 0.331, iii) 0.512, and iv) 0.844

Fig. 8 DLR FLOWer grid, $\alpha = 0$ deg.

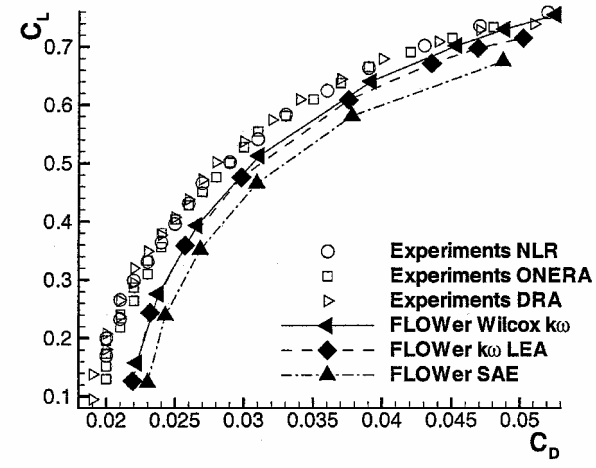

a) $C_L(C_D)$

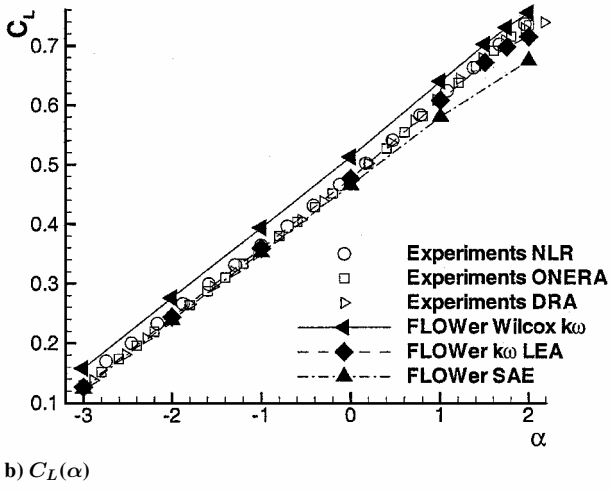

b) $C_L(\alpha)$

Fig. 9 FLOWer on DLR 3.5*e*6 points grid.

are calculated with FLOWer using both the DPW workshop grid (3.2*e*6 nodes) and the DLR grid (3.5*e*6 nodes). With TAU a single point on the polar is computed ($\alpha = 0$) with a hybrid DLR mesh with 2.4*e*6 nodes. In all of the computations, the fixed transition pattern from the experiments is used.[1]

Figure 11 depicts the impact of transition on computed drag, which leads to a reduction in drag of approximately 14 drag counts (or 4%) for the FLOWer computations and 10 drag counts (or 5%) for TAU. All of the structured FLOWer computations use $\zeta = 0.67$ because the only influence of transition being investigated is that which explains the higher level of drag as compared to the FLOWer results using the Wilcox–$k\omega$ model[8] presented earlier.

An important result from these calculations is the difference in drag of approximately 20% between the structured DPW and DLR grids. The parameter settings for the calculations were the same, and the grids are of similar sizes. This clearly demonstrates the effect of mesh quality on drag prediction.

Comparison of FLOWer and TAU and Influence of Geometry Modification

The following sets of results stem from investigations into the cause of the significant differences between the results of the FLOWer and TAU calculations presented in Figs. 4a–5b. The results obtained with the structured solver FLOWer are very good when the influence of transition is considered. Even though the exact cause of these differences has not been located and is a cause for ongoing work, the results of the extensive investigations to date are in and of themselves interesting and worth noting.

The major differences between the computations (apart from the solver and grid types) are the turbulence model, artificial dissipation settings, and the geometry modifications. With respect to the turbulence model, Figs. 9a–10b, show quite clearly that respectable results can be obtained using the SA model.[10] The FLOWer implementation uses the SAE (see Ref. 11) TAU, which is (by default) the original version. A calculation was performed with TAU and the SAE and the differences between the two TAU results are insignificant (as can be expected). Figures 7a–8b show that different settings for the artificial dissipation parameters are also not responsible for the discrepancies between the two codes. Finally, the influence of the geometry modifications in the FLOWer grid have been investigated. The modified surface description used by the MegaCads grid generator, with the closed trailing edge, was read into Centaur™, and two separate hybrid grids were generated. The first grid had a standard O-type prism mesh around the wing (1.3*e*6 points), and the second included a wake panel (the same as used by MegaCads) and, hence, had a C-type mesh around the wing for a better resolution of the wake flow behind the wing (1.7*e*6 points). All other grid generation parameters (for example, number of prism layers, prism layer thickness, etc.) were kept the same to minimize differences in the grid characteristics.

Computations were performed with TAU on both grids, with the results from the grid with the O-type prism mesh and the closed trailing edge being presented in Figs. 12a–13b and compared to the FLOWer SAE (see Ref. 11) results from the section "Influence of Turbulence Modelling in FLOWer" and the TAU results with the original blunt trailing-edge grid from case 2. For these

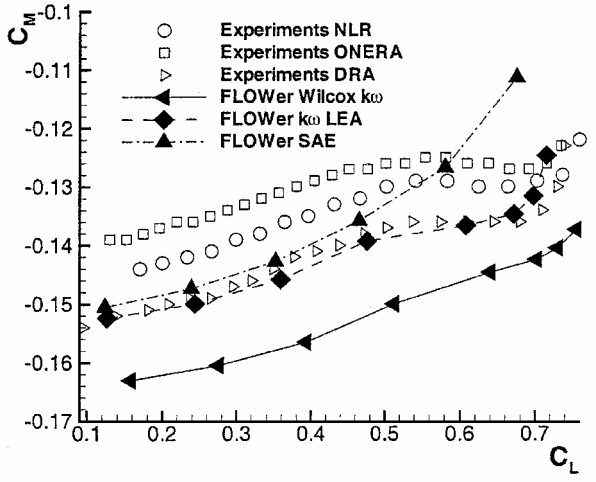

a) $C_M(C_L)$

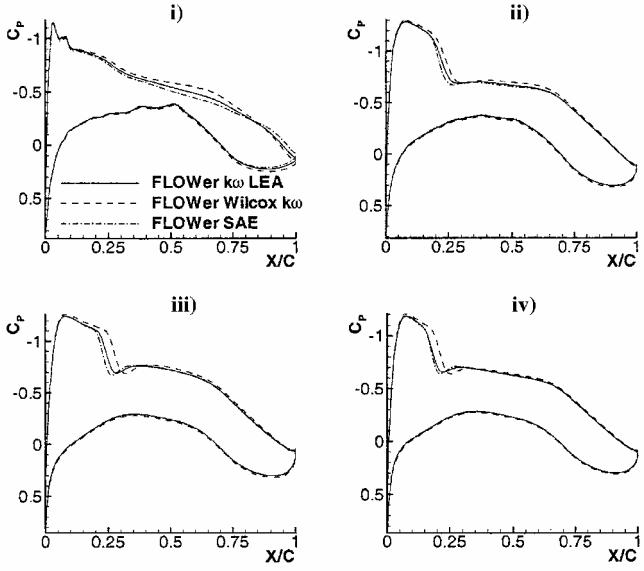

b) $C_P(x/c)$: η = i) 0.185, ii) 0.331, iii) 0.512, and iv) 0.844

Fig. 10 FLOWer on DLR 3.5*e*6 points grid at $\alpha = 0$ deg.

comparisons, the adaptation step was omitted from the additional TAU computations.

In general, it can be concluded that the influence of the geometry modification is negligible, at least when trying to explain the differences between the TAU results and both the results obtained with FLOWer and those of the experiments. The results from the grid with the wake mesh (not shown) also brought no further improvement. The two TAU drag polars in Fig. 12a are almost identical, with a slight shift at the higher values of C_L. The lift over alpha curves in Fig. 12b for the two TAU results are identical for $\alpha = -3$–0 deg, and at higher angles of attack the geometry with the closed trailing edge produces a negligibly higher lift. The general trend, however, remains the same: The unstructured computations overpredict the lift consistently over the whole range of angles of attack. Earlier results have shown that the pitching moment curve is most sensitive to any differences in computational results. Although there is a small difference in the pitching moments (Fig. 13a) between the two TAU grids, it can be concluded that, in general, there are insignificant changes in the computational results for this geometry brought about by the geometry modifications introduced in generating the block structured DLR grid with MegaCads.

Figure 13b shows the respective wing pressure distributions from the three computations at $\alpha = 0$ deg, that is, with a higher C_L than the experiment. This causes an overly optimistic comparison with experiment; however, the differences between the the two TAU computations and the FLOWer result are of interest. The FLOWer result shows a more forward shock position in the three outer sections.

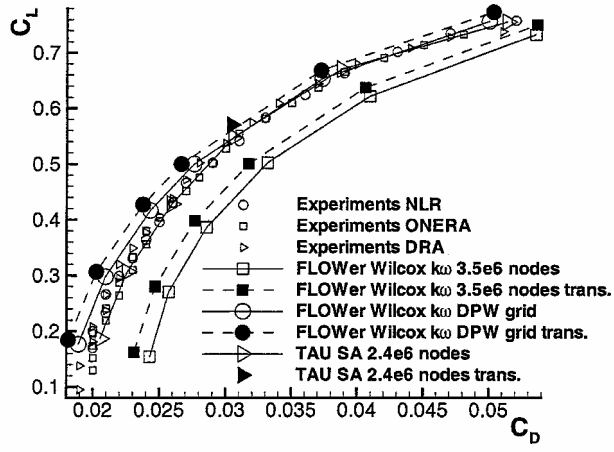

Fig. 11 $C_L(C_D)$ Influence of transition on FLOWer and TAU results on DLR and DPW grids.

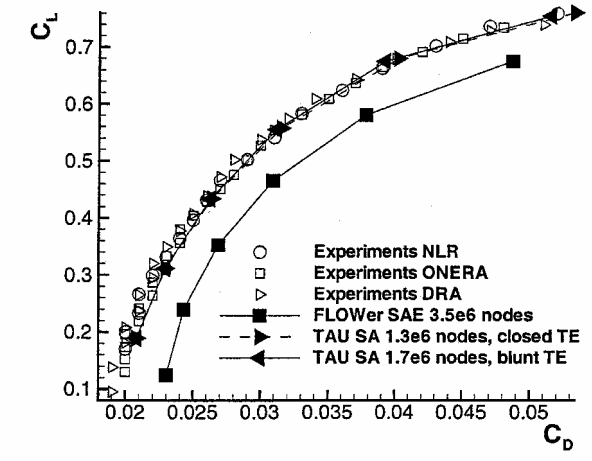

a) $C_L(C_D)$

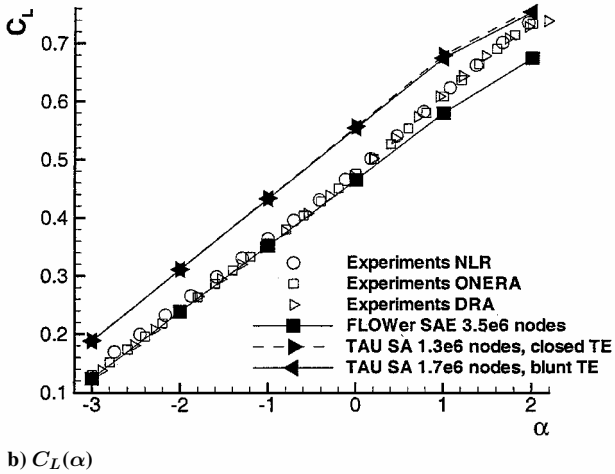

b) $C_L(\alpha)$

Fig. 12 FLOWer and TAU on DLR grids, $\alpha = 0$ deg.

Also, there are differences in the pressure recovery region. The higher lift at the same angle of attack is clearly visible.

For completeness, a final grid modification was tested on the grid with the O-type prismatic mesh and the closed trailing edge. The height of the first cell away from the wall was reduced down to 0.0005 mm and 30 layers were generated in the prismatic part of the mesh (prismatic stretching factor of 1.31) to keep the total height of the prismatic mesh the same. Again, no significant differences were found in any of the computational results.

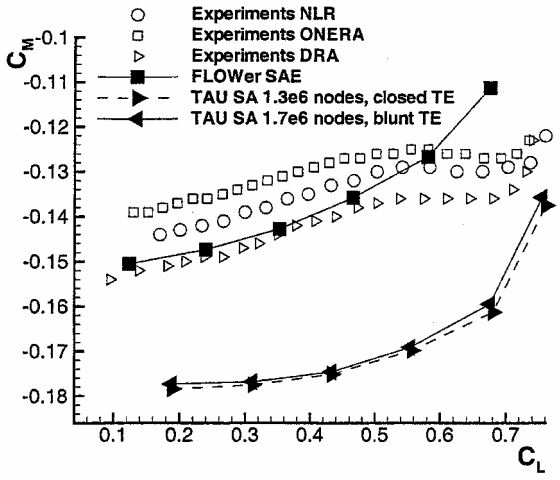

a) $C_M(C_L)$

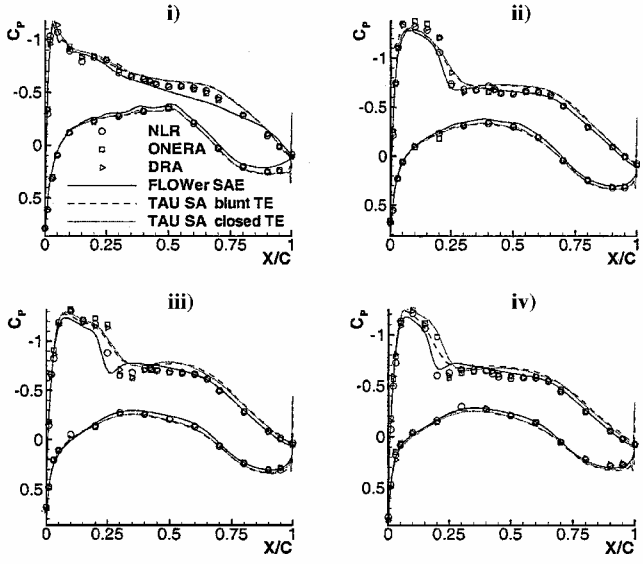

b) $C_P(x/c)$: η = i) 0.185, ii) 0.331, iii) 0.512, and iv) 0.844

Fig. 13 FLOWer and TAU on DLR grids, α = 0 deg.

Influence of Mesh Refinement and Grid Extrapolation for FLOWer

The influence of grid refinement is demonstrated with FLOWer computations using the $k\omega$–LEA turbulence model and the parameter settings for minimal artificial dissipation on three grids with 3.5*e*6, 5*e*6, and 18.7*e*6 nodes. Figure 14 includes complete polars for the two smaller grids and a single point computation on the 18.7*e*6 nodes grid showing the results for the finest level and the result of the successive next coarser level with 2.3*e*6 points. These two grid level results are used for a Richardson extrapolation (see Ref. 16) to estimate the grid-independent drag. The general Richardson extrapolation for the grid-converged value f_0 is

$$f_0 \cong f_1 + (f_1 - f_2)/(r^p - 1) \tag{1}$$

Generally, grid refinement reduces the drag with a parallel shift of the polars. The second-level computation of the 18.7*e*6 points grid is almost identical to the result on the 3.5*e*6 nodes grid. The polar of the 5*e*6 points grid is shifted noticeably to lower drag, indicating grid dependence. The result for the 18.7*e*6 points grid is shifted by a similar amount to lower drag, indicating reduced mesh dependence for finer grids. The fine grid result is on top of the ONERA experiments. The black triangle is the extrapolated value using the theoretical order of accuracy of FLOWer and the grid refinement $r = 2$, which is only slightly shifted to lower drag, indicating a high level of grid independence of the fine grid solution. The extrapolation shows that the grid converged solution, including transition, would lie at a noticeably lower drag level compared to the experiments.

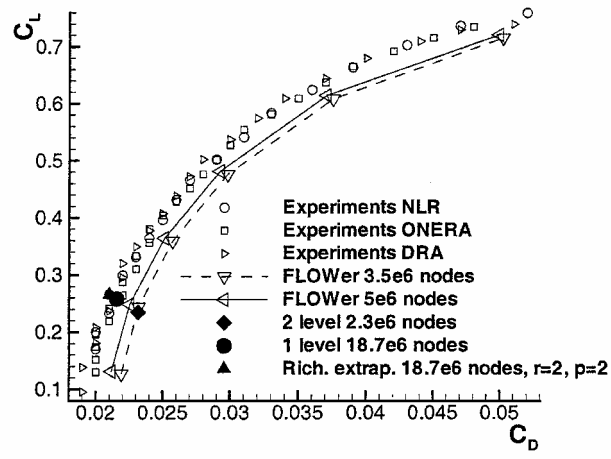

Fig. 14 $C_L(C_D)$ FLOWer on DLR grids.

Conclusions

It is possible to achieve accurate CFD results for transonic flows using a structured grid solver (FLOWer) on a wing–body configuration by the use of a high-quality grid combined with low levels of artificial dissipation and a sophisticated turbulence model ($k\omega$–LEA). If all of these prerequisites are set, global forces and moments agree well with the experiments, as well as pressure distributions. The computational predictions are, however, very grid dependent, with differences in drag of up to 20% being found for two grids of similar size (DPW, 3.2*e*6 points and DLR, 3.5*e*6 points). It is also possible, with a grid of lower quality, to achieve a good prediction for drag, with poor agreement for lift and pitching moment, due to a cancellation of errors effect. Hence, all three forces should be considered in assessing the quality of any computational solution.

On the unstructured side (TAU), it has been shown that qualitatively good results can be currently achieved. However, for this configuration and flowfield, the results are quantitatively not as good as those of the structured grid approach. This is (currently) the price to be paid for the significant reduction in the total time (grid generation and solution time) required to obtain a solution for such a geometry. A comprehensive parameter study investigating the effect of artificial dissipation, transition, grid topology, and geometry modifications has failed to account for the quantitative differences between the unstructured grid results and both the structured grid results and the experiments.

Acknowledgments

This study is a collaboration between the DLR Institute of Aerodynamics and Flow Technology, Braunschweig and Göttingen, Germany and Airbus Deutschland GmbH, Bremen, Germany. The authors wish to thank both organizations for their advice and support, and, in particular, Hans Bleecke and Jens Fassbender. The support from CentaurSoft for the unstructured grid generation is also appreciated.

References

[1]Redeker, G., "DLR-F4 Wing Body Configuration," AR-303, AGARD, 1994, pp. 4.1–4.21.

[2]Gerhold, T., Friedrich, O., Evans, J., and Galle, M., "Calculation of Complex Three-Dimensional Configurations Employing the DLR TAU-Code," AIAA Paper 97-0167, 1997.

[3]Kroll, N., Radespiel, R., and Rossow, C.-C., "Accurate and Efficient Flow Solvers for 3D Applications on Structured Meshes," R-807, AGARD, 1995, pp. 4.1–4.59.

[4]Brodersen, O., Hepperle, M., Ronzheimer, A., Rossow, C.-C., and Schöning, B., "The Parametric Grid Generation System MegaCads," *5th International Conference on Numerical Grid Generation in Computational Fluid Dynamics and Related Fields*, edited by B. K. Soni, J. F. Thompson, J. Häuser, and P. Eisenmann, NSF Engineering Research Center for Computational Field Simulation, College of Engineering, Mississippi State Univ., Mississippi, 1996, pp. 353–362.

[5]Kroll, N., Rossow, C.-C., Becker, K., and Thiele, F., "MEGAFLOW—A Numerical Flow Simulation System," International Council of the Aeronautical Sciences, ICAS-Paper 2.7.4, Sept. 1998.

[6]Monsen, E., and Rudnik, R., "Investigation of the Blunt Trailing Edge Problem for Supercritical Airfoils," AIAA Paper 95-0089, 1995.

[7]Rakowitz, M., *Grid Refinement Study with a UHCA Wing–Body Configuration Using Richardson Extrapolation and Grid Convergence Index GCI*, Vol. 77, Notes on Numerical Fluid Mechanics, Springer-Verlag, Berlin, Heidelberg, New York, 2002.

[8]Wilcox, D. C., *Turbulence Modeling for CFD*, DCW Industries, Inc., La Cañada, CA, 1993, pp. 84–87.

[9]Monsen, E., Franke, M., Rung, T., Aumann, P., and Ronzheimer, A., "Assessment of Advanced Transport-Equation Turbulence Models for Aircraft Aerodynamic Performance Prediction," AIAA Paper 99-3701, 1999.

[10]Spalart, P., and Allmaras, S., "A One-Equation Turbulence Model for Aerodynamic Flows," AIAA Paper 92-0439, 1992.

[11]Edwards, J., and Chandra, S., "Comparison of Eddy Viscosity-Transport Turbulence Models for Three-Dimensional, Shock-Separated Flows," *AIAA Journal*, Vol. 34, No. 4, 1996, pp. 756–763.

[12]Jameson, A., Schmidt, W., and Turkel, E., "Numerical Solutions of the Euler Equations by Finite-Volume Methods Using Runge–Kutta Time-Stepping Schemes," AIAA Paper 81-1259, 1981.

[13]Martinelli, L., and Jameson, A., "Validation of a Multigrid Method for the Reynolds-Averaged Navier–Stokes Equation," AIAA Paper 88-0414, 1988.

[14]Turkel, E., "Improving the Accuracy of Central Difference Schemes," *Proceedings of the 11th International Conference on Numerical Methods in Fluid Dynamics*, *Lecture Notes in Physics*, edited by D. L. Dwoyer, M. Y. Hussaini, and R. G. Voigt, Vol. 323, Springer-Verlag, Berlin, Heidelberg, New York, 1989, pp. 586–591.

[15]Pirzadeh, S., "Three-Dimensional Unstructured Viscous Grids by the Advancing-Layers Method," *AIAA Journal*, Vol. 34, No. 1, 1996, pp. 43–49.

[16]Roache, P., *Verification and Validation in Computational Science and Engineering*, Hermosa, Albuquerque, NM, 1998, p. 109.